

# Exploring the AI Obedience: Why is Generating a Pure Color Image Harder than CyberPunk?

Hongyu Li<sup>\*1</sup>, Kuan Liu<sup>\*2</sup>, Yuan Chen<sup>2</sup>, Juntao Hu<sup>2</sup>, Huimin Lu<sup>2</sup>, Guanjie Chen<sup>3</sup>,  
Xue Liu<sup>4</sup>, Guangming Lu<sup>1</sup>, Hong Huang<sup>†2</sup>

<sup>1</sup>Harbin Institute of Technology, Shenzhen <sup>2</sup>City University of Hong Kong

<sup>3</sup>Chinese University of Hong Kong <sup>4</sup>McGill University

<https://ai-obedience.github.io>

<https://github.com/AI-Obedience/Violin>

<https://huggingface.co/datasets/Perkzi/VIOLIN>

## Abstract

Recent advances in generative AI have demonstrated remarkable ability to produce high-quality content. However, these models often exhibit “Paradox of Simplicity”: while they can render intricate landscapes, they often fail at simple, deterministic tasks. To address this, we formalize Obedience as the ability to align with instructions and establish a hierarchical grading system ranging from basic semantic alignment to pixel-level systemic precision, which provides a unified paradigm for incorporating and categorizing existing literature. Then, we conduct case studies to identify common obedience gaps, revealing how generative priors often override logical constraints. To evaluate high-level obedience, we present VIOLIN (VI<sup>isual</sup> O<sup>bedience</sup> L<sup>evel</sup>-4 E<sup>valuat</sup>Io<sup>N</sup>), the first benchmark focused on pure color generation across six variants. Extensive experiments on SOTA models reveal fundamental obedience limitations and further exploratory insights. By establishing this framework, we aim to draw more attention on AI Obedience and encourage deeper exploration to bridge this gap.

## 1. Introduction

The rapid advancement of generative AI has achieved a significant milestone in producing content at human-level (Karras et al., 2019; Ho et al., 2020; Rombach et al., 2022; Labs et al., 2025; Wu et al., 2025a). These methods have achieved transformative breakthroughs in fields such as image editing (Brooks et al., 2023), programming (Guo et al.,

\*Equal contribution.

†Correspondence Author <honghuang2000@outlook.com>.

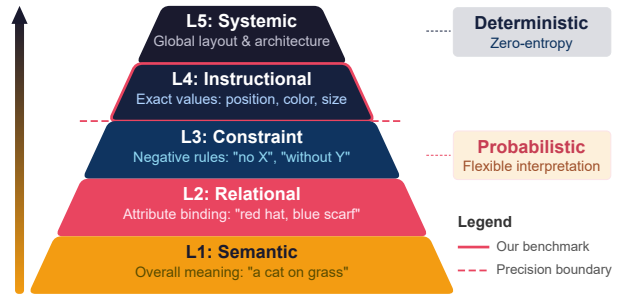


Figure 1. Hierarchy of Proposed Obedience System.

2024; Zhu et al., 2024), and conversational document analysis (Grattafiori et al., 2024), boosting daily and professional efficiency. However, although achievement, the current generative AI creates a “Paradox of Simplicity”: models that can render complex landscapes often fail at trivial tasks. For example, most AI failed to generate a pure color image, always tend to add objects, noise, or textures. We argue that this phenomenon is not a random error, but a critical and systemic failure case. To comprehensively investigate this issue, we introduce the **Obedience**: a model’s fundamental capacity to align its generative behavior with explicit user constraints, particularly the ability to suppress generative instincts when a deterministic output is required.

This raises a fundamental question: *Why is generating a pure RGB(255, 0, 0) image harder for AI than a “Cyberpunk Cityscape”?* We identify the core issue as **Aesthetic Interference**, where the model’s internal criteria for image quality inevitably introduce texture or lighting that conflict with simple, deterministic instructions. Current generative models excel at low-level obedience (e.g. semantic), capturing the overall meaning or “vibe” of a prompt, but fail at Instructional(Deterministic) Obedience, which requires exact pixel-level control. This distinction is critical for prac-

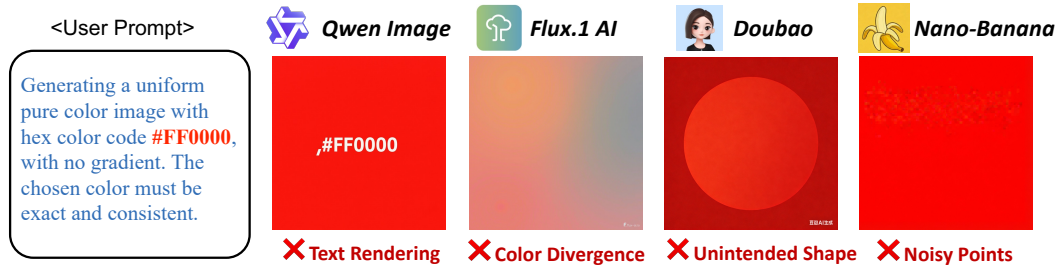


Figure 2. **Visualization of instruction-following failures** in pure color generation. Instead of adhering strictly to input instructions, models reflexively introduce spurious artifacts and gradients, highlighting a critical bottleneck in precise generative control.

tical applications. First, deterministic control is essential for safety: if identical prompts yield unpredictable results, AI systems cannot be trusted in automated pipelines. Second, in domains like medical imaging, any deviation from instructions introduces data corruption. For instance, if a model is asked to “mark all regions with density above threshold X in pure red” but adds shading for visual appeal, it injects false information into diagnostic data. High obedience ensures outputs faithfully reflect input specifications without artificial embellishment.

To formalize these issues, we propose the AI Obedience Level Systems from conceptual approximation to numerical exactness: Level 1 (Semantic Obedience) and Level 2 (Relational Obedience) focus on content alignment, ensuring the model captures the correct categories and binding correct attributes. Level 3 (Constraint Obedience) introduces a phase shift: *inhibition*. Here, the model must control its generative priors to follow negative constraints. Level 4 (Instructional Obedience) and Level 5 (Systemic Obedience) represent the transition to “pixel-level determinism”, where the model must treat the output not as a probabilistic image, but as a rigid data structure governed by numerical values or coordinates. Beyond limiting creativity, the concept of Obedience requires the model to strictly follow a prompt: executing instructions with requested accuracy, while retaining flexibility only when allowed for open-ended generation.

Existing research has predominantly concentrated on Level 1 ~ 2, while higher-level obedience remains largely unexplored. In this work, we focus on pure color generation, which shifts to precise pixel-to-pixel control. This task offers a unique structural advantage: for any given input, there exists a non-entropy ground-truth: the exact target pixel value. By removing the ambiguity of generative tasks, this setup provides a deterministic test case where the model’s adherence can be measured with certainty.

To evaluate high-level obedience, we introduce the VIOLIN benchmark, designed to measure how strictly a model adheres to precise color constraints on Level 4. We propose six challenging variations: variation 1 assesses single-color; variations 2 ~ 3 evaluate spatial layout obedience across

two and four colors; variation 4 tests obedience under vague color ranges; variation 5 examines cross-lingual obedience through multilingual prompts; and variation 6 evaluates adherence to other color systems. Our metric focuses on two core dimensions of obedience: color precision, which measures how closely the output matches the target *RGB* values, and color purity, which quantifies the model’s ability to resist generating extraneous noise or textures.

Overall, the primary contributions of this work are threefold:

- **Obedience Concept and Framework:** We are the first to formalize the concept of AI Obedience, establishing a hierarchical grading system with Level 0 ~ 5. Within this framework, we conduct case studies to present key observations and formulate hypotheses.
- **A High-Level Visual Obedience Benchmark:** To bridge the gap in high-level evaluation, we introduce VIOLIN, the first systematic benchmark dedicated to Level 4 Obedience. This includes a dataset featuring six variations and a dual-metric suite measuring color precision and color purity.
- **Empirical Analysis and Discovery:** Through extensive experiments, we find that existing models struggle with high-level obedience. Our results indicate that increasing task-specific data alone cannot fully bridge this gap, highlighting the inherent challenge.

## 2. Obedience and Problems

### 2.1. Definition of Obedience

In the pursuit of Artificial Generative Intelligence (AGI), the focus is shifting from specialized task solvers to versatile, general-purpose systems. However, as these models gain increasing autonomy and generative power, controllability emerges as a fundamental prerequisite for their integration into real-world workflows, where unpredictable outputs can lead to significant functional failures. To emphasize a controllability concept that contrasts with current research trends, which often prioritize creative diversity over strict adherence, we introduce the concept of **Obedience**.

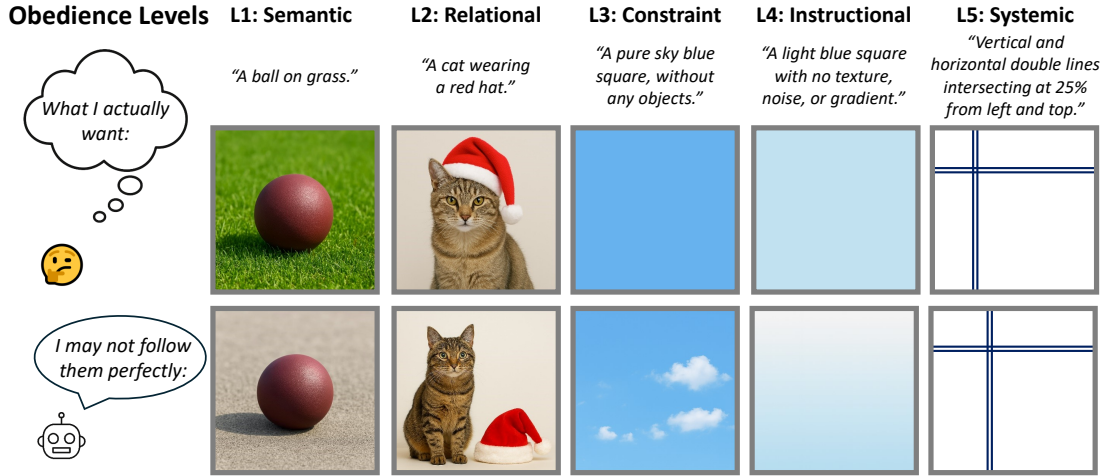


Figure 3. Illustration of obedience levels in image generation. Each column shows the prompt, the expected output, and a failure case, demonstrating how violations correspond to different obedience level definitions.

This term is designed to characterize the degree to which model outputs precisely execute input instructions, serving as a rigorous metric for the reliability of AGI systems in following human intent.

**Definition 2.1. Obedience:** Let  $\mathcal{M} : \mathcal{I} \rightarrow \mathcal{P}(\mathcal{O})$  be a generative model that maps an instruction space  $\mathcal{I}$  to a probability distribution  $\mathcal{P}(\cdot)$  over the output space  $\mathcal{O}$ . For an instruction  $I \in \mathcal{I}$  at level  $L \in \{1, \dots, 5\}$ , the **Obedience Score** is defined by a level-specific operator, which consists of a suite of specialized metrics designed to verify the various constraints required at that level:

$$\text{Obedience}_{\mathcal{M}}(I, L) = \Phi_L(\mathbb{P}_{\mathcal{M}|I}, f_L^*(I)) \quad (1)$$

where  $\mathbb{P}_{\mathcal{M}|I}$  denotes the output distribution generated by the model given instruction  $I$ ,  $f_L^*(I)$  defines the oracle mapping for instruction  $I$ , representing the deterministic ground-truth output that perfectly satisfies the constraints of level  $L$ . This formulation unifies different evaluation granularities:

- **Per-instance level:**  $\Phi_L$  acts as a metric  $d(o, o^*)$  between a single sample  $o \sim \mathbb{P}_{\mathcal{M}|I}$  and the target  $f_L^*(I)$ .
- **Distribution level:**  $\Phi_L$  measures the divergence between the generated distribution  $\mathbb{P}_{\mathcal{M}|I}$  and a target distribution to account for generative stochasticity.

## 2.2. Obedience Levels

To provide a rigorous framework for evaluating generative systems, we propose a grading system of AI Obedience standard. This hierarchy characterizes the transition from probabilistic approximation to deterministic execution, centered on the model’s ability to govern its generative priors.

### Level 0: Non-Obedience

The model ignores the user’s intent. Whether the instruction

is general or specific, the model follows only its internal training data and fails to acknowledge the prompt.

- ◊ *Criterion:* When the instruction is general or ambiguous, the model ignores the prompt’s constraints and produces unrelated output.

### Level 1: Semantic Obedience (“Vibe” Level)

At this level, obedience is defined by the alignment between the instruction’s broad intent and the output semantic.

- ◊ *Criterion:* For general or low-constraint instructions, the model must map broad conceptual requirements to a valid representation within the output domain.
- ◊ *Failure Mode:* The output falls outside the intended conceptual boundaries, resulting in a mismatch with the prompt’s intent (e.g., unrelated objects, incorrect task types, or irrelevant domains)

### Level 2: Relational Obedience (“Binding” Level)

At this level, obedience is defined by maintaining the integrity of multi-entity instructions, ensuring that specific attributes and relational constraints are correctly localized.

- ◊ *Criterion:* For complex or high-constraint prompts, the model must accurately bind independent properties to their respective subjects and respect relative positioning or logical associations.
- ◊ *Failure Mode:* Properties or relations migrate between entities, resulting in a structural mismatch (e.g., mismatched attributes, swapped roles, or inverted spatial/logical relationships).

### Level 3: Constraint Obedience (“Inhibition” Level)

At this level, obedience is defined by the model’s capacity to follow restrictive or negative constraints by intentionally suppressing its internal priors.

- ◇ *Criterion*: For exclusionary or minimalist prompts, the model must filter out prohibited elements and maintain a strict adherence to the specified limitations.
- ◇ *Failure Mode*: The model introduces unrequested attributes (e.g., adding decorative textures, stylistic nuances, or extra logic) to avoid a simplistic output.

#### Level 4: Instructional Obedience (Deterministic Level)

At this level, obedience is defined by the elimination of stochastic variance within the output’s fundamental units. The model must treat the output space as a rigid data structure, ensuring that every discrete element aligns perfectly with the specified numerical parameters.

- ◇ *Criterion*: For accurate (or parameterized) instruction, the model must achieve zero-entropy mapping (e.g., exact color values or bit-perfect consistency) where the output signal is a 1:1 reflection of the instruction.
- ◇ *Failure Mode*: Subtle fluctuations (e.g., pixel-level noise or value variance) that prevent the output from reaching a pure, mathematically certain state.

#### Level 5: Systemic Obedience (“Architectural” Level)

The highest level of obedience represents the total alignment of generative capacity with complex geometric or logical specifications. The model operates as a high-fidelity rendering engine, strictly adhering to absolute coordinates and rigid structural interdependencies.

- ◇ *Criterion*: For coordinate-based or blueprint-style prompts, the model must ensure geometric exactness and dimensional accuracy, verifiable through external measurement tools.
- ◇ *Failure Mode*: Misalignment of coordinates or structural warping (e.g., an entity appearing at coordinates (120, 120) instead of the requested (100, 100)).

This hierarchy reveals a fundamental shift in how we evaluate generative AI by drawing a clear line between. We define this critical boundary as the “Exact Alignment Threshold”: *Beyond Level 3, the model transitions from probabilistic interpretation to deterministic execution, achieving the ability to map input instructions to output details with zero-variance precision.*

**Relation to Existing Concepts:** Obedience serves as a unified framework that categorizes existing evaluation standards based on the strictness of the instructions. We category current benchmarks and metrics as follows:

- **Level-1:** Recent benchmarks include DrawBench (Saharia et al., 2022) and PAINTSKILLS (Cho et al., 2023), alongside foundational alignment metrics such as CLIPScore (Radford et al., 2021) BLIPScore (Li et al., 2022), Semantic Object Accuracy (Hinz et al., 2020) and VIdoCon(Bansal et al., 2024).

- **Level-2:** Benchmarks like VISOR (Gokhale et al., 2022), T2I-CompBench (Huang et al., 2023), TIFA (Hu et al., 2023), and SeeTrue (Yarom et al., 2023), alongside metrics including SR-Score (Huang et al., 2023) for spatial logic, TIAM (Grimal et al., 2024) for attribute binding, and TIFA-Count (Hu et al., 2023) for numerical accuracy.

- **Level-3** A representative benchmark is **NEG-TTOI** (Cai et al., 2025), which evaluates “Not-to-Generate” scenarios.

### 2.3. Pure Color Generation Task

To systematically investigate obedience, we prioritize evaluation tasks with uniquely determined outputs that allow for direct quantification of instruction-execution precision. Unlike text generation, which inherently suffers from randomness in wording and expression, visual tasks provide much stronger output constraints when parameters such as resolution are fixed, despite the remaining degrees of freedom in natural scene composition.

We therefore select the most fundamental and elementary task in the visual domain—**Pure Color Generation**—as our starting point. This task requires to generate uniform images of specified colors, providing an ideal experimental paradigm for quantitative obedience analysis.

### 2.4. Diagnosing the High-Level Obedience

To identify the bottlenecks in achieving high-level obedience, we identify three aspects: Negation, Semantic Gravity, and Aesthetic Inertia in pure color generation task. We conduct experiments using Qwen-Image.

#### 2.4.1. THE EFFECT OF NEGATION

This study examines the model’s capacity for Logical Inhibition within the pure color task. Specifically, we investigate whether the model can utilize negative prompts to suppress unintended color interference.

- $P_{\text{base}}^1$ : A simple, positive instruction providing only the hex code (“*Generating a uniform pure color image with hex color code: #9966CC.*”)
- $P_{\text{neg}}^1$ : Introducing strict negative constraints targeting high-probability textures for gray (“*..., strictly no shadows, no gradients, and no metallic textures.*”)
- $P_{\text{ent}}^1$ : Using terms that are semantically distant but visually noisy (“*..., strictly no cloud patterns or water ripples.*”)

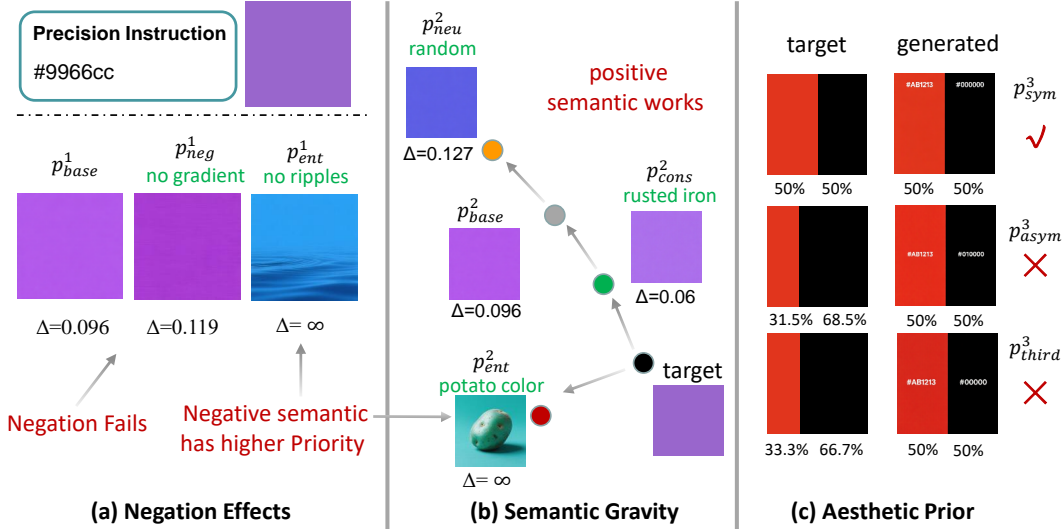


Figure 4. **Diagnostic case studies** (a) Logical Inhibition Failure: Negative prompts (“no gradient”) fail to remove artifacts, and mentioning semantic object to avoid (“ripples”) causes the model to generate them instead. (b) Semantic Gravity: The model follows color instructions better when they align with common knowledge (“rusty iron”), but drifts when the context is conflicting or random. (c) Aesthetic Inertia: Precise spatial ratios (31.5%) are ignored in favor of a standard 50/50 symmetrical split.

As illustrated in Figure 4 (a),  $P_{base}^1$  yields a lighter color, but adding negative constraints in  $P_{neg}^1$  actually worsens the result. Most notably,  $P_{ent}^1$  leads the model to directly generate visual ripples despite being told to avoid them.

#### 2.4.2. THE “SEMANTIC GRAVITY”

This study investigates when numerical instructions are subjected to varying semantic contexts, a phenomenon we term “Semantic Gravity.” We examine whether the model maintains numerical fidelity or drifts toward the semantic center of the surrounding text.

- $P_{base}^2$ : the same as  $P_{1,base}$ .
- $P_{cons}^2$ : associate with a consistent prior testing if aligned priors can act as an anchor to improve precision. (“..., which is the typical color of a rusted iron plate”),
- $P_{conf}^2$ : associate with a conflicting prior to measure the “pull” of training data distributions. (“..., representing the color of a fresh potato”)
- $P_{neu}^2$ : Explicitly stripping semantic meaning to observe if logical de-biasing can mitigate aesthetic interference. (“..., a randomly generated color with no specific meaning or real-world counterpart”)

As illustrated in Fig 4(b),  $P_{cons}^2$  shows that aligning the color with a familiar prior (“rusty iron”) acts as an anchor that improves precision. In contrast,  $P_{conf}^2$  causes the model to generate a physical “potato” instead of the requested color,

while  $P_{neu}^2$  (random) actually leads to worse performance.

#### 2.4.3. SPATIAL PRECISION VS. AESTHETIC BIAS

This study investigates the conflict between precise spatial layout and “Aesthetic Inertia”, the tendency to favor balanced, conventional compositions over exact numerical ratios. We test whether the model can execute spatial instructions when they deviate from common visual patterns:

- $P_{sym}^3$ : A standard balanced split (“A split image with two solid color blocks: the left 50% is a pure solid color with hex code #AB1213, the right 50% is a pure solid color with hex code #000000”).
- $P_{asym}^3$ : A non-standard, precise ratio (“A split image with two solid color blocks: the left 31.5% is a pure solid color with hex code #AB1213, the right 68.5% is a pure solid color with hex code #000000”).
- $P_{third}^3$ : A common photographic composition (“A common photographic composition with two solid color blocks: the left 33.3% is a pure solid color with hex code #AB1213, the right 66.7% is a pure solid color with hex code #000000”).

As shown in Fig 4(c), even asked for specific ratios like 31.5%, the model defaults to a balanced 50/50 split.

#### 2.4.4. SUMMARY OF OBSERVATIONS AND HYPOTHESES.

Our case studies reveal that high-level obedience is bottlenecked by a tension between explicit logic and implicit visual priors. We formalize these findings into three hypotheses: **Priority of Semantic Priming over Logical Inhibition**: The positive activation of a visual concept (e.g., “ripples”) dominates the inhibitory signal of negative constraints (e.g., “no”), causing the model to generate the features it was told to avoid. **Semantic Gravity Effect**: Numerical precision is not processed as abstract logic but is “pulled” toward dense clusters in the training distribution, causing drift toward familiar semantic anchors. **Aesthetic Inertia**: Persistent layout biases, such as symmetrical 50/50 splits, usually overrides precise spatial ratios. Collectively, these phenomena suggest that SOTA models act as *intuitive artists* rather than precision tools, prioritizing associative visual coherence over the rigorous execution of logical instructions.

### 3. VIOLIN Benchmark

#### 3.1. Datasets

To bridge the gap in existing research regarding high-level obedience, we propose the first benchmark specifically designed to assess Level-4: **VIOLIN (VIsual Obedience Level-4 EvaluatIoN)**. Focused on pure color generation, VIOLIN serves as an evaluation tool to push the boundaries of current obedience research. The dataset consists of text-image pairs where the ground truth is programmatically synthesized; every pixel maintains the strictly requested values, establishing a deterministic standard that eliminates visual ambiguity. To this end, the benchmark is organized into six variations through distinct dimensions:

**Variation 1: Single Color Block** As the basic scenario, we consider the task where the entire image consists of a single uniform color, using diverse prompt templates to cover various textual expressions. To encompass color descriptions at multiple granularities, we adopt hexadecimal color code representations based on the ISCC-NBS system.

**Variation 2/3: Multi-Color Block** As an extension of variation 1, we construct multi-color block tasks to evaluate models’ ability to handle scenarios with color contrasts. Specifically, variation 2 corresponds to two-color blocks (horizontal or vertical split), and variation-3 corresponds to four-color blocks (2×2 grid), as they provide unambiguous spatial partitioning, whereas other configurations such as 3-color blocks introduce spatial layout ambiguity.

**Variation 4: Fuzzy Color** Building on the variation-1 scenario, we provide an acceptable color range rather than exact values to evaluate model obedience under fuzzy constraints. This variation systematically assesses how models handle instruction-following precision when given flexible

yet bounded color specifications.

**Variation 5: Multilingual Prompts** To evaluate model obedience across diverse linguistic systems, we extend the variation-1 to Chinese and French, representing logographic and Latin-based writing systems respectively. This expansion allows us to investigate whether differences in grammatical structure, color vocabulary, and cultural context impact the model’s precision in executing color-related instructions.

**Variation 6: Multiple Color Space** To assess the impact of color encoding, we extend the single-color task to include RGB and HSL formats alongside hex codes. This expansion allows us to investigate whether varying mathematical foundations across these representation methods introduce specific biases or affect the model’s depth of understanding.

#### 3.2. Evaluation Metrics

To quantify the degree of Obedience, we evaluate model performance through two dimensions: **Color Precision** and **Color Purity**. Color Precision utilizes a dual-color-space strategy to quantify the deviation between generated and target colors. Color Purity captures unintended visual artifacts, such as irregular textures and inconsistent gradients. In both dimensions, higher scores indicate worse obedience.

**Color Precision** We evaluate on two color spaces: RGB for measuring direct digital pixel alignment, and CIE  $L^*a^*b^*$  (CIELAB) for perceptual alignment. By decomposing color into luminance and chromaticity, CIELAB provides a perceptually uniform metric where Euclidean distances correspond to human discrimination thresholds.

In RGB space, we employ two distance metrics: (1) Euclidean Distance ( $d_{rgb.ed}$ ): computes the Euclidean distance across three RGB channels, providing the most intuitive measure; (2) RedMean Distance ( $d_{rgb.rm}$ ): Considering the sensitivity of human eyes to the RGB channels, this metric adaptively adjusts the weights of each channel to provide a calculation more aligned with human visual perception:

$$\begin{aligned}\bar{r} &= \frac{1}{2}(R_1 + R_2), \\ c_1 &= \left(2 + \frac{\bar{r}}{256}\right) \\ c_3 &= \left(2 + \frac{255 - \bar{r}}{256}\right) \\ d_{rgb.rm} &= \sqrt{c_1\Delta R^2 + 4\Delta G^2 + c_3\Delta B^2}.\end{aligned}\tag{2}$$

where  $\Delta R = R_1 - R_2$ ,  $\Delta G = G_1 - G_2$ ,  $\Delta B = B_1 - B_2$ .

In Lab space, we employ four metrics: (1) CIEDE2000 ( $d_{lab.00}$ ): as the standard evaluation method, this metric employs complex nonlinear transformations and incorporates weighting functions to more accurately model human visual system perceptual characteristics; (2) Mae Hue

## Exploring the Obedience Limit with Pure Color Generation Benchmark

**Table 1. Comparison of Level-4 Obedience across Variation 1-3.** We evaluate models on the full benchmark to assess their ability to accurately synthesize colors under increasing complexity. "Color Precision" and "Color Purity" metrics are reported, where lower values indicate better performance. The best and second-best results in each category are highlighted in **red** and **blue**, respectively.

Var	Models	Color Precision ↓						Color Purity ↓				
		rgb-ed	rgb-rm	lab-00	lab-hue	lab-hyab	lab-ch	pre-mean	sd	ced	hf	pur-mean
Var-1	SANA	0.288	0.284	0.331	0.375	0.145	0.477	0.319	0.232	0.028	0.030	0.097
	Janus-Pro-1.5	0.344	0.343	0.410	0.561	0.169	0.527	0.396	0.193	0.006	0.004	0.068
	FLUX.1	0.364	0.357	0.387	0.403	0.159	0.469	0.356	0.044	<b>0.001</b>	<b>0.001</b>	<b>0.015</b>
	Qwen-Image	0.156	0.153	0.180	0.206	0.077	0.246	0.171	0.058	<b>0.002</b>	0.021	0.027
	OmniGen2	0.397	0.390	0.402	0.449	0.178	0.526	0.390	0.202	0.070	0.016	0.096
	Nano-Banana	<b>0.111</b>	<b>0.108</b>	<b>0.104</b>	<b>0.091</b>	<b>0.050</b>	<b>0.149</b>	<b>0.102</b>	<b>0.011</b>	<b>0.001</b>	<b>0.001</b>	<b>0.004</b>
	Seedream-4.5	0.198	0.193	0.208	0.246	0.091	0.277	0.203	0.215	0.013	0.023	0.083
GPT-Image-1.5	<b>0.054</b>	<b>0.053</b>	<b>0.053</b>	<b>0.050</b>	<b>0.026</b>	<b>0.080</b>	<b>0.053</b>	<b>0.013</b>	0.030	<b>0.001</b>	<b>0.015</b>	
Var-2	SANA	0.315	0.308	0.352	0.396	0.157	0.531	0.346	0.312	0.019	0.021	0.118
	Janus-Pro-1.5	0.335	0.327	0.359	0.511	0.155	0.480	0.365	0.216	0.009	0.012	0.079
	FLUX.1	0.357	0.353	0.384	0.448	0.165	0.490	0.367	<b>0.117</b>	<b>0.005</b>	<b>0.005</b>	<b>0.042</b>
	Qwen-Image	0.128	0.125	0.143	0.177	0.065	0.216	0.143	<b>0.111</b>	0.007	0.028	<b>0.049</b>
	OmniGen2	0.388	0.382	0.396	0.419	0.185	0.572	0.390	0.236	0.036	0.026	0.099
	Nano-Banana	<b>0.113</b>	<b>0.111</b>	<b>0.107</b>	<b>0.105</b>	<b>0.052</b>	<b>0.157</b>	<b>0.107</b>	0.226	<b>0.005</b>	<b>0.005</b>	0.079
	Seedream-4.5	0.201	0.195	0.218	0.286	0.096	0.294	0.216	0.421	0.018	0.043	0.161
GPT-Image-1.5	<b>0.056</b>	<b>0.055</b>	<b>0.056</b>	<b>0.061</b>	<b>0.027</b>	<b>0.086</b>	<b>0.057</b>	0.265	<b>0.001</b>	<b>0.002</b>	0.089	
Var-3	SANA	0.369	0.360	0.401	0.442	0.187	0.642	0.403	0.433	0.030	0.035	0.166
	Janus-Pro-1.5	0.338	0.334	0.383	0.514	0.160	0.476	0.370	0.220	0.022	0.024	0.089
	FLUX.1	0.386	0.379	0.416	0.473	0.189	0.602	0.409	<b>0.142</b>	<b>0.008</b>	<b>0.008</b>	<b>0.053</b>
	Qwen-Image	0.229	0.224	0.264	0.333	0.115	0.371	0.258	<b>0.174</b>	0.015	0.029	<b>0.073</b>
	OmniGen2	0.410	0.405	0.433	0.465	0.204	0.631	0.425	0.242	0.024	0.025	0.097
	Nano-Banana	<b>0.122</b>	<b>0.119</b>	<b>0.114</b>	<b>0.113</b>	<b>0.055</b>	<b>0.161</b>	<b>0.114</b>	0.338	0.009	0.011	0.120
	Seedream-4.5	0.211	0.203	0.226	0.305	0.100	0.306	0.227	0.520	0.023	0.053	0.199
GPT-Image-1.5	<b>0.073</b>	<b>0.071</b>	<b>0.075</b>	<b>0.083</b>	<b>0.035</b>	<b>0.108</b>	<b>0.074</b>	0.364	<b>0.004</b>	<b>0.006</b>	0.125	

( $d_{lab.hue}$ ): maps colors to the hue in cylindrical coordinates (0-360 degrees) and directly computes hue angle differences;  
(3) Delta Chroma ( $d_{lab.ch}$ ): Quantifies only chroma (color vividness/saturation) differences while isolating the influence of lightness variations:

$$d_{lab.ch} = \sqrt{(a_2 - a_1)^2 + (b_2 - b_1)^2} \quad (3)$$

(4) Delta E HyAB ( $d_{lab.hyab}$ ): combines both chroma and lightness simultaneously, incorporates lightness to provide a more comprehensive assessment of perceptual color differences when substantial changes occur.

$$d_{lab.hyab} = \sqrt{(a_2 - a_1)^2 + (b_2 - b_1)^2 + |L_2 - L_1|} \quad (4)$$

**Color Purity** To evaluate visual elements that deviate from pure colors, such as noise, textures, and unintended shapes, we design three metrics. Notably, this requires no ground truth reference but directly quantifies the uniformity of a single image: (1) Standard Deviation ( $d_{sd}$ ): compute the standard deviation across all channels; (2) Canny Edge Density ( $d_{ced}$ ): employ the canny algorithm to detect edge features and calculate the proportion of edge pixels relative to the total number of pixels. This metric is sensitive to intensity variations, suitable for assessing the structural textures or shapes; (3) High-Frequency Component Ratio

( $d_{hf}$ ): transform the image to the frequency domain via 2D Fast Fourier Transform (2D FFT) and compute the energy ratio of high-frequency components. This corresponds to fine details and rapid variations, enabling to capture subtle purity defects such as minor noise and local color discrepancies.

**Metric Integration** To integrate individual metrics, we normalize each metric to the [0,1] interval, and compute the mean precision and mean purity as unified metrics:

$$\begin{aligned} d_{pre.mean} &= w_1 * \hat{d}_{rgb.ed} + w_2 * \hat{d}_{rgb.rm} \\ &+ w_3 * \hat{d}_{lab.00} + w_4 * \hat{d}_{lab.hue} \\ &+ w_5 * \hat{d}_{lab.hyab} + w_6 * \hat{d}_{lab.ch} \\ d_{pur.mean} &= w_7 * \hat{d}_{sd} + w_8 * \hat{d}_{ced} + w_9 * \hat{d}_{hf} \end{aligned} \quad (5)$$

where hat indicates that variable has been normalized.

## 4. Experiments

### 4.1. Implementation

**Models** To conduct comprehensive evaluation, we choose recent state-of-the-art visual generation models, covering both open-source and closed-source, as well as T2I architectures and unified multimodal designs. The open-source models include SANA (Xie et al., 2024a), Janus-Pro-1.5 (Chen

Table 2. **Performance after fine-tuning.** Models are trained on a subset of the **variation 1** data to ensure rigorous results. Compared to the Var-1 in Table 1, the performance shifts are inconsistent: some show better ( $\downarrow$ ), some remain unchanged( $-$ ), some show worse ( $\uparrow$ ).

Models	Color Precision $\downarrow$							Color Purity $\downarrow$			
	rgb-ed	rgb-rm	lab-00	lab-hue	lab-hyab	lab-ch	pre-mean	sd	ced	hf	pur-mean
SANA	0.292	0.288	0.330	0.374	0.144	0.462	0.317 $-$	0.211	0.00	0.027	0.085 $\downarrow$
Janus-Pro-1.5	0.090	0.088	0.121	0.182	0.051	0.172	0.119 $\downarrow$	0.010	0.001	0.001	0.004 $\downarrow$
FLUX.1	0.227	0.223	0.283	0.412	0.117	0.377	0.277 $\downarrow$	0.004	0.000	0.001	0.001 $\downarrow$
Qwen-Image	0.167	0.166	0.208	0.326	0.087	0.288	0.210 $\uparrow$	0.018	0.001	0.001	0.006 $\downarrow$
OmniGen2	0.413	0.407	0.412	0.437	0.177	0.501	0.391 $-$	0.159	0.060	0.014	0.078 $\downarrow$

Table 3. **Generalization ability analysis.** Evaluating the model’s zero-shot generalization on three designed color partition strategies.

Models	Color Precision $\downarrow$							Color Purity $\downarrow$			
	rgb-ed	rgb-rm	lab-00	lab-hue	lab-hyab	lab-ch	pre-mean	sd	ced	hf	pur-mean
Prompt-Split	0.095	0.093	0.113	0.147	0.048	0.159	0.110	0.048	0.004	0.010	0.021
Hue-Split1	0.127	0.124	0.156	0.231	0.066	0.216	0.155	0.023	0.003	0.002	0.009
Hue-Split2	0.128	0.126	0.158	0.243	0.065	0.206	0.156	0.034	0.003	0.004	0.014

et al., 2025), OmniGen2 (Wu et al., 2025b), FLUX.1 (Labs et al., 2025), and Qwen-Image(Wu et al., 2025a); the closed-source models include GPT-Image-1.5, Seedream-4.5 (Seedream et al., 2025), and Nano-Banana-Pro.

#### 4.2. Visual Level-4 Obedience Evaluation

To investigate the Level-4 Obedience of existing models, we evaluate all candidates on the full benchmark, with the results summarized in Table 1. It demonstrate that that closed-source models generally exhibit superior color precision compared to open-source models. As the complexity scales from Var-1 to Var-3, we observe a consistent performance degradation across both metrics. Notably, Nano-Banana and GPT-Image-1.5 emerge as the top performers, maintaining low error rates even in the difficult scenarios.

It is worth noting that most existing models are primarily optimized for natural scene rather than explicit color precision. To ensure a rigorous evaluation, we finetune the open-source models, as shown in Table 2. Interestingly, a comparison with the Var-1 baseline in Table 1 shows that while color purity (pur-mean) generally improves across most models, the shifts in color precision (pre-mean) are inconsistent. We hypothesize that these varying responses are rooted in the different training priors, simple fine-tuning may not serve as a universal solution for improving color obedience across all existing architectures.

#### 4.3. Generalization Evaluation

Since the above experiments provide only a coarse-grained analysis, we conduct fine-grained evaluations of model generalization in color obedience. We design three data partition strategies: (1) prompt-based partitioning(Prompt-Split): splitting data by template to evaluate different instruction

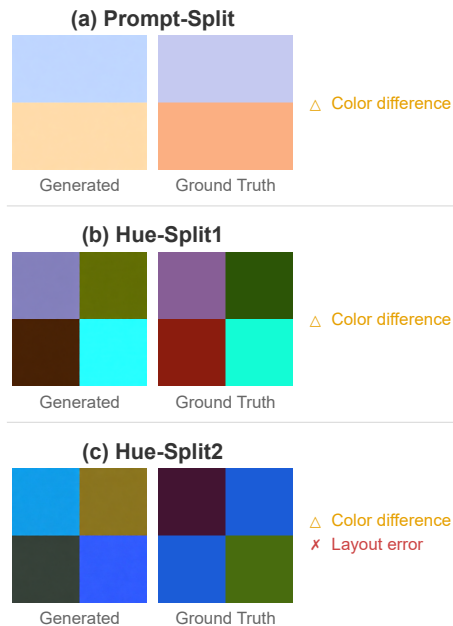


Figure 5. **Generalization Results.** All cases show color difference, while (c) also shows layout inaccuracies.

formulations; (2) localized hue partitioning(Hue-Split1): testing purple range ( $280^{\circ}$ - $320^{\circ}$  hue) while training on the remainder; (3) distributed hue partitioning(Hue-Split2)): training on three distributed ranges ( $0^{\circ}$ - $60^{\circ}$ ,  $120^{\circ}$ - $180^{\circ}$ ,  $240^{\circ}$ - $300^{\circ}$ ) with the rest for testing.

As shown in Table 3, while color purity generalizes across different setting, color precision exhibits bad performance. We hypothesize that current models may rely more on the memorization rather than developing a truly robust understanding of the color space, shown in Fig 5.

## 5. Conclusion

In this paper, we have explored the “Paradox of Simplicity” in generative AI and formalize the concept of Obedience, establishing a hierarchical grading system. Our proposed VIOLIN benchmark, focused on Level-4 Obedience through pure color generation task, offers an effective evaluation and explorative tool. Our investigation through case studies and extensive experiments reveals that current models often prioritize generative priors over logical constraints. While our benchmark demonstrates the utility of certain models, we observe that high-level obedience cannot be achieved solely through exposure to task-specific data, suggesting a need for structural improvements. By establishing this framework, we hope to draw more attention to AI Obedience and encourage the development of next-generation models that are not only “creative artists” but also “precise executors”.

## Impact Statement

This paper presents work whose goal is to advance the field of deep learning and Generative AI. There are many potential societal consequences of our work, none which we feel must be specifically highlighted here.

## References

- Bansal, H., Bitton, Y., Szpektor, I., Chang, K.-W., and Grover, A. Videocon: Robust video-language alignment via contrast captions. In *Proceedings of the IEEE/CVF Conference on Computer Vision and Pattern Recognition*, pp. 13927–13937, 2024.
- Binyamin, L., Tewel, Y., Segev, H., Hirsch, E., Rassin, R., and Chechik, G. Make it count: Text-to-image generation with an accurate number of objects. In *Proceedings of the Computer Vision and Pattern Recognition Conference*, pp. 13242–13251, 2025.
- Brooks, T., Holynski, A., and Efros, A. A. Instructpix2pix: Learning to follow image editing instructions. In *Proceedings of the IEEE/CVF conference on computer vision and pattern recognition*, pp. 18392–18402, 2023.
- Butt, M. A., Wang, K., Vazquez-Corral, J., and van de Weijer, J. Colorpeel: Color prompt learning with diffusion models via color and shape disentanglement. In *European Conference on Computer Vision*, pp. 456–472. Springer, 2024.
- Cai, Y., Thomason, J., and Rostami, M. Tng-clip: Training-time negation data generation for negation awareness of clip. *arXiv preprint arXiv:2505.18434*, 2025.
- Chen, X., Wu, Z., Liu, X., Pan, Z., Liu, W., Xie, Z., Yu, X., and Ruan, C. Janus-pro: Unified multimodal understanding and generation with data and model scaling. *arXiv preprint arXiv:2501.17811*, 2025.
- Cho, J., Zala, A., and Bansal, M. Dall-eval: Probing the reasoning skills and social biases of text-to-image generation models. In *Proceedings of the IEEE/CVF international conference on computer vision*, pp. 3043–3054, 2023.
- Esser, P., Kulal, S., Blattmann, A., Entezari, R., Müller, J., Saini, H., Levi, Y., Lorenz, D., Sauer, A., Boesel, F., et al. Scaling rectified flow transformers for high-resolution image synthesis. In *Forty-first international conference on machine learning*, 2024.
- Gokhale, T., Palangi, H., Nushi, B., Vineet, V., Horvitz, E., Kamar, E., Baral, C., and Yang, Y. Benchmarking spatial relationships in text-to-image generation. *arXiv preprint arXiv:2212.10015*, 2022.

- Goodfellow, I., Pouget-Abadie, J., Mirza, M., Xu, B., Warde-Farley, D., Ozair, S., Courville, A., and Bengio, Y. Generative adversarial networks. *Communications of the ACM*, 63(11):139–144, 2020.
- Grattafiori, A., Dubey, A., Jauhri, A., Pandey, A., Kadian, A., Al-Dahle, A., Letman, A., Mathur, A., Schelten, A., Vaughan, A., et al. The llama 3 herd of models. *arXiv preprint arXiv:2407.21783*, 2024.
- Grimal, P., Le Borgne, H., Ferret, O., and Tourille, J. Tiam-a metric for evaluating alignment in text-to-image generation. In *Proceedings of the IEEE/CVF Winter Conference on Applications of Computer Vision*, pp. 2890–2899, 2024.
- Guo, D., Zhu, Q., Yang, D., Xie, Z., Dong, K., Zhang, W., Chen, G., Bi, X., Wu, Y., Li, Y., et al. Deepseek-coder: When the large language model meets programming—the rise of code intelligence. *arXiv preprint arXiv:2401.14196*, 2024.
- Hinz, T., Heinrich, S., and Wermter, S. Semantic object accuracy for generative text-to-image synthesis. *IEEE transactions on pattern analysis and machine intelligence*, 44(3):1552–1565, 2020.
- Ho, J. and Salimans, T. Classifier-free diffusion guidance. *arXiv preprint arXiv:2207.12598*, 2022.
- Ho, J., Jain, A., and Abbeel, P. Denoising diffusion probabilistic models. *Advances in neural information processing systems*, 33:6840–6851, 2020.
- Hu, Y., Liu, B., Kasai, J., Wang, Y., Ostendorf, M., Krishna, R., and Smith, N. A. Tifa: Accurate and interpretable text-to-image faithfulness evaluation with question answering. In *Proceedings of the IEEE/CVF International Conference on Computer Vision*, pp. 20406–20417, 2023.
- Huang, K., Sun, K., Xie, E., Li, Z., and Liu, X. T2i-compbench: A comprehensive benchmark for open-world compositional text-to-image generation. *Advances in Neural Information Processing Systems*, 36:78723–78747, 2023.
- Jiang, D., Ku, M., Li, T., Ni, Y., Sun, S., Fan, R., and Chen, W. Genai arena: An open evaluation platform for generative models. *Advances in Neural Information Processing Systems*, 37:79889–79908, 2024.
- Karras, T., Laine, S., and Aila, T. A style-based generator architecture for generative adversarial networks. In *Proceedings of the IEEE/CVF conference on computer vision and pattern recognition*, pp. 4401–4410, 2019.
- Kingma, D. P. and Welling, M. Auto-encoding variational bayes. *arXiv preprint arXiv:1312.6114*, 2013.
- Labs, B. F., Batifol, S., Blattmann, A., Boesel, F., Consul, S., Diagne, C., Dockhorn, T., English, J., English, Z., Esser, P., et al. Flux. 1 kontext: Flow matching for in-context image generation and editing in latent space. *arXiv preprint arXiv:2506.15742*, 2025.
- Li, B., Lin, Z., Pathak, D., Li, J., Fei, Y., Wu, K., Ling, T., Xia, X., Zhang, P., Neubig, G., et al. Genai-bench: Evaluating and improving compositional text-to-visual generation. *arXiv preprint arXiv:2406.13743*, 2024a.
- Li, J., Li, D., Xiong, C., and Hoi, S. Blip: Bootstrapping language-image pre-training for unified vision-language understanding and generation. In *International conference on machine learning*, pp. 12888–12900. PMLR, 2022.
- Li, L., Wei, Y., Xie, Z., Yang, X., Song, Y., Wang, P., An, C., Liu, T., Li, S., Lin, B. Y., et al. VI-rewardbench: A challenging benchmark for vision-language generative reward models. In *Proceedings of the Computer Vision and Pattern Recognition Conference*, pp. 24657–24668, 2025.
- Li, Z., Cheng, T., Chen, S., Sun, P., Shen, H., Ran, L., Chen, X., Liu, W., and Wang, X. Controlar: Controllable image generation with autoregressive models. *arXiv preprint arXiv:2410.02705*, 2024b.
- Liang, Y., Li, M., Fan, C., Li, Z., Nguyen, D., Cobbina, K., Bhardwaj, S., Chen, J., Liu, F., and Zhou, T. Colorbench: Can vlms see and understand the colorful world? a comprehensive benchmark for color perception, reasoning, and robustness. *arXiv preprint arXiv:2504.10514*, 2025.
- Radford, A., Kim, J. W., Hallacy, C., Ramesh, A., Goh, G., Agarwal, S., Sastry, G., Askell, A., Mishkin, P., Clark, J., et al. Learning transferable visual models from natural language supervision. In *International conference on machine learning*, pp. 8748–8763. PmLR, 2021.
- Ramesh, A., Dhariwal, P., Nichol, A., Chu, C., and Chen, M. Hierarchical text-conditional image generation with clip latents. *arXiv preprint arXiv:2204.06125*, 1(2):3, 2022.
- Rombach, R., Blattmann, A., Lorenz, D., Esser, P., and Ommer, B. High-resolution image synthesis with latent diffusion models. In *Proceedings of the IEEE/CVF conference on computer vision and pattern recognition*, pp. 10684–10695, 2022.
- Saharia, C., Chan, W., Saxena, S., Li, L., Whang, J., Denton, E. L., Ghasemipour, K., Gontijo Lopes, R., Karagol Ayan, B., Salimans, T., et al. Photorealistic text-to-image diffusion models with deep language understanding. *Advances in neural information processing systems*, 35: 36479–36494, 2022.

- Seedream, T., Chen, Y., Gao, Y., Gong, L., Guo, M., Guo, Q., Guo, Z., Hou, X., Huang, W., Huang, Y., et al. Seedream 4.0: Toward next-generation multimodal image generation. *arXiv preprint arXiv:2509.20427*, 2025.
- Shum, K. C., Hua, B.-S., Nguyen, D. T., and Yeung, S.-K. Color alignment in diffusion. In *Proceedings of the Computer Vision and Pattern Recognition Conference*, pp. 28446–28455, 2025.
- Team, C. Chameleon: Mixed-modal early-fusion foundation models. *arXiv preprint arXiv:2405.09818*, 2024.
- Wu, C., Li, J., Zhou, J., Lin, J., Gao, K., Yan, K., Yin, S.-m., Bai, S., Xu, X., Chen, Y., et al. Qwen-image technical report. *arXiv preprint arXiv:2508.02324*, 2025a.
- Wu, C., Zheng, P., Yan, R., Xiao, S., Luo, X., Wang, Y., Li, W., Jiang, X., Liu, Y., Zhou, J., et al. Omnigen2: Exploration to advanced multimodal generation. *arXiv preprint arXiv:2506.18871*, 2025b.
- Xie, E., Chen, J., Chen, J., Cai, H., Tang, H., Lin, Y., Zhang, Z., Li, M., Zhu, L., Lu, Y., et al. Sana: Efficient high-resolution image synthesis with linear diffusion transformers. *arXiv preprint arXiv:2410.10629*, 2024a.
- Xie, J., Mao, W., Bai, Z., Zhang, D. J., Wang, W., Lin, K. Q., Gu, Y., Chen, Z., Yang, Z., and Shou, M. Z. Show-o: One single transformer to unify multimodal understanding and generation. *arXiv preprint arXiv:2408.12528*, 2024b.
- Xu, J., Liu, X., Wu, Y., Tong, Y., Li, Q., Ding, M., Tang, J., and Dong, Y. Imagereward: Learning and evaluating human preferences for text-to-image generation. *Advances in Neural Information Processing Systems*, 36: 15903–15935, 2023.
- Yarom, M., Bitton, Y., Changpinyo, S., Aharoni, R., Herzig, J., Lang, O., Ofek, E., and Szepes, I. What you see is what you read? improving text-image alignment evaluation. *Advances in Neural Information Processing Systems*, 36:1601–1619, 2023.
- Zhang, L., Rao, A., and Agrawala, M. Adding conditional control to text-to-image diffusion models. In *Proceedings of the IEEE/CVF international conference on computer vision*, pp. 3836–3847, 2023.
- Zhu, Q., Guo, D., Shao, Z., Yang, D., Wang, P., Xu, R., Wu, Y., Li, Y., Gao, H., Ma, S., et al. Deepseek-coder-v2: Breaking the barrier of closed-source models in code intelligence. *arXiv preprint arXiv:2406.11931*, 2024.

## A. Related Work

**Generative Models in Visual Domain** Unlike the open-ended nature of text, the pixel-level determinism in visual generation makes it an ideal testbed for evaluating fine-grained instruction obedience. Capitalizing on this potential, visual generation, particularly image generation, has witnessed remarkable progress, with models now capable of synthesizing highly complex scenes that demand precise control. In text-to-image (T2I) generation, diffusion models (Ho et al., 2020; Ramesh et al., 2022) have surpassed conventional generative approaches such as GAN (Goodfellow et al., 2020) and VAE (Kingma & Welling, 2013) by learning Gaussian denoising through reverse diffusion processes. Models such as Stable Diffusion (Rombach et al., 2022; Esser et al., 2024), FLUX (Labs et al., 2025), and Qwen-Image (Wu et al., 2025a) have demonstrated exceptional performance with expanding training data and model scales. Besides, unified models integrating multimodal understanding and visual generation have also emerged as a prominent research direction. Several studies adopt autoregressive (AR) frameworks analogous to LLMs (Team, 2024), while others investigate hybrid architectures combining diffusion and AR (Xie et al., 2024b) to leverage complementary strengths of both paradigms. These models have achieved great breakthroughs in vision-language alignment and multi-modal generation tasks.

**Low-Level AI Obedience** Existing research focuses on low-level visual obedience at the Semantic (Level-1) and Relational (Level-2) tiers. To achieve Level-1, foundational mechanisms like Classifier-Free Guidance (CFG) (Ho & Salimans, 2022) and ControlNet (Zhang et al., 2023) enforce alignment via latent guidance and spatial-semantic priors, while ImageReward (Xu et al., 2023) utilizes human preference learning to refine semantic fidelity. Level-2 research further improves attribute-object binding, using precise color codes (Butt et al., 2024), reference images (Shum et al., 2025), or specialized modules to associate textures and quantities without attribute leakage (Li et al., 2024b; Binyamin et al., 2025). However, these methods prioritize visual “naturalness” over perfect “accuracy”, lacking the strict pixel-level control required for deterministic, zero-variance alignment with user specifications.

**Obedience Benchmarks** Multiple benchmarks have been proposed to evaluate the obedience of generative models across various dimensions. In terms of semantic and relational understanding, comprehensive suites like T2I-CompBench (Huang et al., 2023) and GenAI-Bench (Li et al., 2024a) assess models’ abilities in multi-object association, counting, and attribute binding. Regarding color specifically, some works design to evaluate the generation or reasoning ability of color in natural scenes (Liang et al., 2025). However, these benchmarks primarily assess low-level obedience, where visual plausibility often lack true precision. They fail to evaluate the model’s ability to prioritize strict instructions over its internal generative priors, which remains the focus of our study.

While recent benchmarks like VLRewardBench (Li et al., 2025) and GenAI Arena (Jiang et al., 2024) evaluate broad instruction-following and alignment, they primarily focus on semantic or aesthetic preferences. VIOLIN complements these by targeting the Level-4 Obedience limit—deterministic, zero-entropy pixel control—which remains a critical failure mode not captured by existing reward-based or arena-style evaluations.

## B. Implementation Details

### Training Details

**Paradigms** We evaluate models under two paradigms. First, all models are directly tested on the full benchmark. Second, to assess learning capabilities on color tasks, we conduct fine-tuning experiments using an 8:2 random train-test split. For open-source models, we apply LoRA for parameter-efficient fine-tuning over 3,000 steps to avoid overfitting. Closed-source models are evaluated only through direct inference via official APIs, as fine-tuning is unavailable.

For fine-tuning experiments, we primarily report results on Qwen-Image with the following configuration.

**LoRA Configuration.** We apply LoRA (Low-Rank Adaptation) for parameter-efficient fine-tuning with rank  $r = 16$ ,  $\alpha = 32$ , and dropout rate of 0.1. LoRA modules are applied to the attention projection matrices (`to_k`, `to_q`, `to_v`, and `to_out.0`). The base model is quantized to `qfloat8` to reduce memory consumption.

**Optimization.** We use the 8-bit AdamW optimizer with a learning rate of  $3 \times 10^{-4}$  and a constant learning rate schedule without warmup. Gradient clipping is applied with a maximum norm of 1.0.

**Training Configuration.** Training is conducted on 4 GPUs with a per-device batch size of 8, resulting in an effective batch size of 32. Models are trained for 3,000 steps with `bf16` mixed precision.

Table 4. Representative prompt examples for each variation in VIOLIN

Variation	Example Prompt
1	Generate an image with pure color #D9B451 (Hex code).
2	Specified in Hex code, produce a background divided horizontally into two equal halves: top color #72672C and bottom color #D9B451.
3	Specified in Hex code, generate an image divided into four quadrants: top-left color #7F4829, top-right color #B92842, bottom-left color #7F4829, bottom-right color #3B74C0. No gradients or shadows.
4	Specified in Hex code, generate an image in a single solid color within the range of #58321D and #A65E35.
5	生成一张颜色为 #B92842 (十六进制代码) 的纯色图像。
6	Generate a plain background using color rgb(217, 180, 81).

Table 5. **Fine-tuning analysis on the Qwen-Image model.** Results report the performance after fine-tuning the model individually on each complexity variation (Variation 1–6).

Models	Color Precision ↓							Color Purity ↓			
	rgb-ed	rgb-rm	lab-00	lab-hue	lab-hyab	lab-ch	pre-mean	sd	ced	hf	pur-mean
Variation-1	0.093	0.092	0.124	0.173	0.052	0.173	0.120	0.023	0.001	0.001	0.010
Variation-2	0.088	0.086	0.110	0.146	0.048	0.161	0.108	0.027	0.003	0.005	0.012
Variation-3	0.163	0.160	0.186	0.230	0.078	0.237	0.177	0.042	0.006	0.005	0.018
Variation-4	0.237	0.220	0.266	0.506	0.115	0.465	0.307	0.052	0.001	0.003	0.019
Variation-5	0.103	0.102	0.140	0.194	0.057	0.199	0.135	0.023	0.001	0.004	0.009
Variation-6	0.190	0.186	0.227	0.286	0.097	0.320	0.220	0.011	0.001	0.001	0.003

**Data Processing.** All training images are resized to  $384 \times 384$  resolution. We precompute and cache text embeddings and image latents to accelerate training. A caption dropout rate of 0.1 is applied for regularization.

**Other Models.** For other models (SANA, Janus-Pro-1.5, OmniGen2, FLUX.1), we use the same LoRA configuration ( $r = 16$ ,  $\alpha = 32$ , dropout=0.1) and effective batch size of 32.

## C. Benchmark Details.

### C.1. Datasets

The VIOLIN dataset is constructed by combining six variations of prompt design with three levels of color granularity derived from the ISCC-NBS system. Across the six variations, we design a total of 100 prompt templates (10, 20, 30, 10, 20, and 10 respectively), ensuring coverage of diverse linguistic and structural forms. Examples are shown in Table 4.

For single-color scenarios (Variation 1), the dataset contains 3,020 text–image pairs, a scale matched by the fuzzy-color setting (Variation 4), each language in the multilingual extension (Variation 5), and each format in the multiple color-space extension (Variation 6). In multi-color block tasks, the dataset expands due to combinatorial expansion: the two-block configuration (Variation 2) yields 12,080 pairs, while the four-block configuration (Variation 3) produces 18,120 pairs.

All images are programmatically synthesized at a fixed resolution of  $256 \times 256$  pixels, with every pixel strictly adhering to the requested specification. The dataset is divided into training and testing subsets with an 8:2 ratio, using stratified sampling to preserve distribution across variations and color levels. In total, VIOLIN comprises over 42,000 text–image pairs.

### C.2. Metrics

**Multi-Block Metric** For multi-color blocks cases, direct application of the above metrics would introduce evaluation bias, as the expected color boundaries and regional variations would be identified as defects. To mitigate this, we employ a block-wise evaluation strategy: the multi-color block image is first partitioned into uniform segments by color regions, metrics are then computed independently for each sub-region, and the results are averaged to yield the final image score.

## Exploring the Obedience Limit with Pure Color Generation Benchmark

Table 6. Comparison of Level-4 Obedience across Variation 4-6. We evaluate models on the full benchmark to assess their ability to accurately synthesize colors under increasing complexity. “Color Precision” and “Color Purity” metrics are reported, where lower values indicate better performance. The best and second-best results in each category are highlighted in red and blue, respectively.

Var	Models	Color Precision ↓						Color Purity ↓				
		rgb-ed	rgb-rm	lab-00	lab-hue	lab-hyab	lab-ch	pre-mean	sd	ced	hf	pur-mean
Var-4	SANA	0.321	0.309	<b>0.367</b>	<b>0.492</b>	0.166	0.594	<b>0.379</b>	0.202	0.048	0.017	0.089
	Janus-Pro-1.5	<b>0.281</b>	<b>0.281</b>	0.380	0.610	0.171	<b>0.561</b>	0.388	<b>0.086</b>	0.005	<b>0.004</b>	<b>0.031</b>
	FLUX.1	0.336	0.326	0.382	<b>0.513</b>	0.166	0.565	0.385	<b>0.062</b>	<b>0.001</b>	<b>0.001</b>	<b>0.021</b>
	Qwen-Image	<b>0.280</b>	<b>0.261</b>	<b>0.303</b>	0.531	<b>0.137</b>	<b>0.532</b>	<b>0.345</b>	0.123	<b>0.004</b>	0.018	0.048
	OmniGen2	0.384	0.371	0.400	0.498	<b>0.165</b>	0.672	0.420	0.132	0.042	0.017	0.064
Var-5(C)	SANA	<b>0.304</b>	<b>0.297</b>	<b>0.344</b>	<b>0.352</b>	0.154	0.528	<b>0.332</b>	0.178	0.041	<b>0.011</b>	<b>0.077</b>
	Janus-Pro-1.5	0.340	0.334	0.373	0.580	<b>0.149</b>	<b>0.423</b>	0.369	0.468	<b>0.025</b>	<b>0.013</b>	0.168
	FLUX.1	0.415	0.411	0.397	0.411	0.170	0.453	0.373	0.529	0.105	0.051	0.228
	Qwen-Image	<b>0.145</b>	<b>0.142</b>	<b>0.178</b>	<b>0.207</b>	<b>0.075</b>	<b>0.250</b>	<b>0.168</b>	<b>0.081</b>	<b>0.005</b>	<b>0.013</b>	<b>0.033</b>
	OmniGen2	0.397	0.391	0.414	0.446	0.187	0.568	0.401	<b>0.173</b>	0.051	0.015	0.080
Var-5(F)	SANA	<b>0.306</b>	<b>0.299</b>	<b>0.342</b>	<b>0.391</b>	<b>0.149</b>	<b>0.478</b>	<b>0.329</b>	<b>0.257</b>	0.031	0.041	0.110
	Janus-Pro-1.5	0.343	0.337	0.382	0.539	0.169	0.525	0.386	0.389	<b>0.014</b>	<b>0.015</b>	0.139
	FLUX.1	0.372	0.368	0.390	0.395	0.170	0.507	0.367	0.267	0.020	0.016	<b>0.101</b>
	Qwen-Image	<b>0.161</b>	<b>0.159</b>	<b>0.201</b>	<b>0.227</b>	<b>0.088</b>	<b>0.305</b>	<b>0.192</b>	<b>0.051</b>	<b>0.002</b>	<b>0.007</b>	<b>0.020</b>
	OmniGen2	0.428	0.420	0.431	0.461	0.208	0.662	0.435	0.379	0.116	0.024	0.173
Var-6(rgb)	SANA	<b>0.331</b>	<b>0.323</b>	<b>0.383</b>	0.426	0.174	0.588	0.374	0.381	0.061	0.034	0.158
	Janus-Pro-1.5	0.343	0.339	0.406	0.540	0.171	0.538	0.393	0.250	<b>0.003</b>	0.005	0.086
	FLUX.1	0.359	0.352	0.394	<b>0.402</b>	<b>0.170</b>	0.536	<b>0.370</b>	0.153	<b>0.001</b>	<b>0.002</b>	0.052
	Qwen-Image	<b>0.212</b>	<b>0.206</b>	<b>0.221</b>	<b>0.245</b>	<b>0.097</b>	<b>0.293</b>	<b>0.212</b>	<b>0.063</b>	<b>0.001</b>	0.009	<b>0.025</b>
	OmniGen2	0.427	0.429	0.447	0.494	0.191	<b>0.510</b>	0.416	<b>0.056</b>	0.012	<b>0.001</b>	<b>0.023</b>
Var-6(hsl)	SANA	<b>0.339</b>	<b>0.332</b>	<b>0.387</b>	0.443	0.173	0.579	0.378	0.335	0.052	0.027	0.138
	Janus-Pro-1.5	0.355	0.346	0.396	0.563	0.171	0.575	0.404	0.264	0.007	0.006	0.092
	FLUX.1	0.366	0.358	0.388	<b>0.392</b>	<b>0.164</b>	<b>0.498</b>	<b>0.361</b>	0.139	<b>0.003</b>	<b>0.002</b>	0.048
	Qwen-Image	<b>0.314</b>	<b>0.303</b>	<b>0.346</b>	<b>0.371</b>	<b>0.167</b>	0.587	<b>0.351</b>	<b>0.102</b>	<b>0.004</b>	0.007	<b>0.037</b>
	OmniGen2	0.374	0.367	0.394	0.424	0.176	<b>0.530</b>	0.377	<b>0.103</b>	0.034	<b>0.003</b>	<b>0.047</b>

**Fuzzy-Color Metric** When prompts specify a color range rather than a single target value, the application of single-block metrics requires an additional reference definition. To resolve this ambiguity, the representative color of the generated image (obtained via mean pooling across pixels) is projected onto the line segment connecting the two boundary colors in HSL space. Formally, given the representative color  $v$  and the boundary colors  $c_{low}$  and  $c_{high}$ , the projection is defined as:

$$t = \frac{(v - c_{low}) \cdot (c_{high} - c_{low})}{\|c_{high} - c_{low}\|^2}, \quad p = c_{low} + t(c_{high} - c_{low}), \quad t \in [0, 1] \quad (6)$$

where  $p$  denotes the nearest point on the segment. This ensures a valid reference color within the specified range. Once this reference is determined, all subsequent computations follow the same pipeline as the single-block metric.

## D. More Experiments

### D.1. Additional Visual Level-4 Obedience Evaluation

As illustrated in Table 6, our evaluation across Variations 4-6 reveals several key findings. Qwen-Image emerges as the dominant performer in nearly all scenarios, maintaining a significant lead in **pre-mean** scores. In contrast, other open-source models exhibit similar but subpar performance, struggling to meet the precision requirements of high-level obedience. Regarding multilingual scenarios, most models achieve their peak performance within English contexts; however, Qwen-Image uniquely realizes its best results in Chinese, suggesting a more robust cross-lingual alignment for instruction following. Furthermore, in terms of color identifiers, we observe that most models perform best with Hex codes, demonstrating that the choice of color representation influences model performance.

### D.2. Evaluation on Each Variations

To compare the performance across variations, we conducted a set of experiments which were trained using the same hyperparameter settings. For variation 1, 4 ~ 6, the training splits were kept identical to eliminate potential effects of data partitioning on performance differences. The results are shown in Table 5.

Taking the variation 1 as the baseline, the multi-block task(variation 2-3) yields similar results, suggesting that comparing colors within a single image may not pose a challenge for current models. However, the fuzzy color span(variation 4) leads to much worse performance, and variations in languages(variation 5) or color representations(variation 6) also result in a noticeable degradation in precision. These interesting findings indicate that different linguistic grammars and information encoding methods may influence the color obedience of Generative AI, which could inspire the further research.

### D.3. Fine-tuning Dynamics on Qwen-Image

To provide a more detailed view of the fine-tuning process, we visualize the training dynamics of Qwen-Image in Figure 6. The top row illustrates how the Color Difference Mean and Color Purity Mean evolve across checkpoints, with the red dashed line indicating the base model’s performance. The bottom row presents a detailed comparison of individual metrics between the base model and the final checkpoint (ckpt3000).

As training progresses, color purity improves rapidly and consistently, while color precision exhibits more volatile behavior with slower convergence. This asymmetry suggests that suppressing visual artifacts (e.g., noise, textures) is a relatively easier objective for the model to learn, whereas achieving precise color matching requires overcoming deeper representational biases embedded in the pretrained weights.

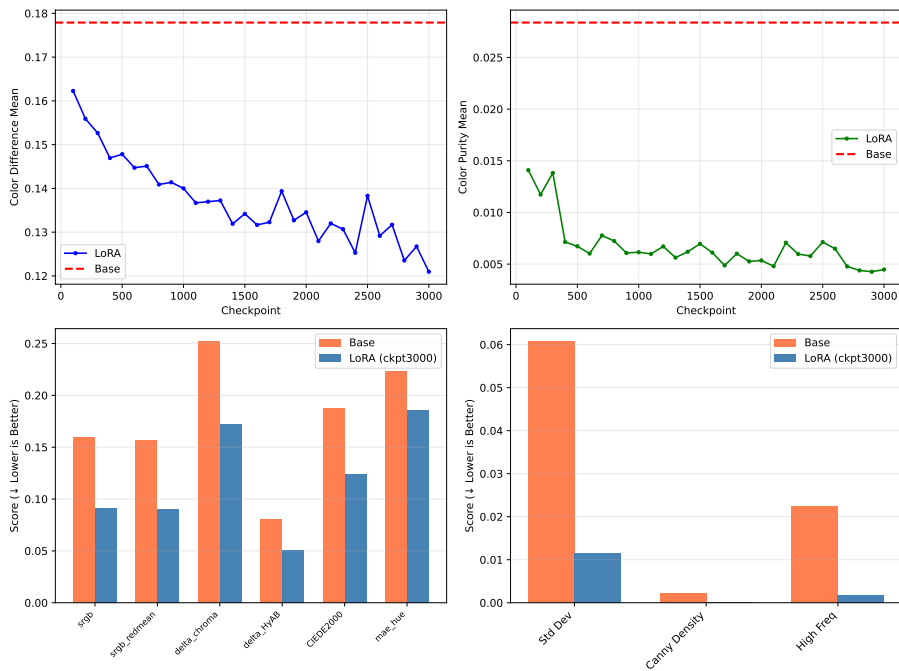


Figure 6. Fine-tuning dynamics of Qwen-Image. Top: training curves for Color Difference Mean and Color Purity Mean. Bottom: detailed metric comparison between the base model and ckpt3000.

### D.4. Qualitative Results

Figure 7 presents representative examples of color generation results from our experiments. Each pair displays the generated output alongside its corresponding ground truth.

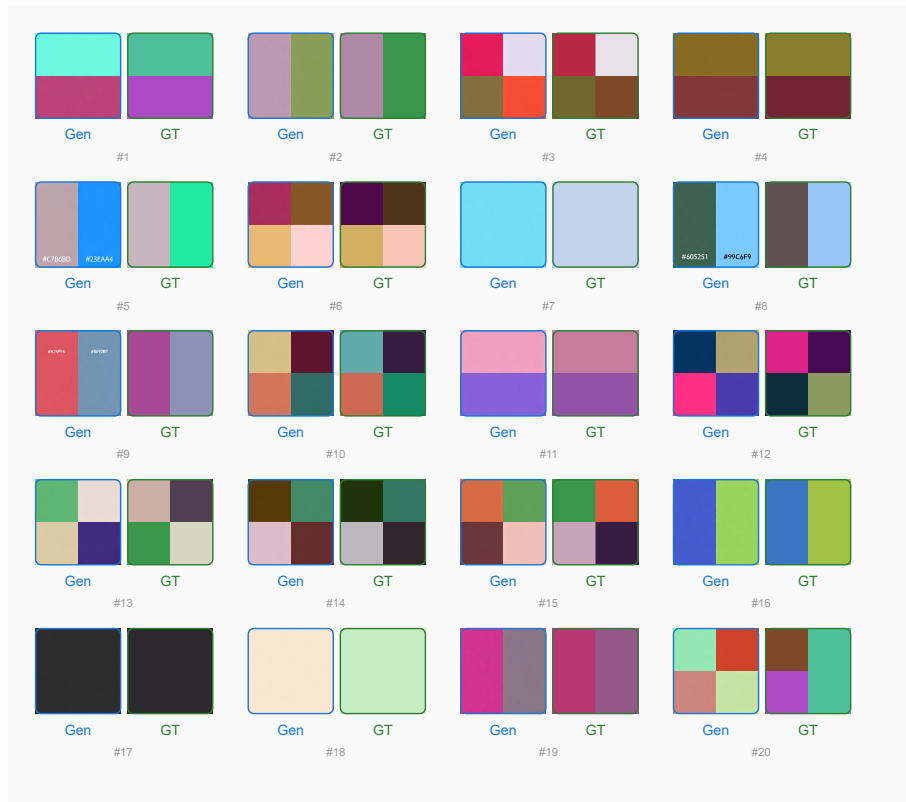


Figure 7. Examples of generated colors (Gen) and ground truth (GT).

## E. Discussions

**The Atomic Nature of Pure Color Obedience.** We intentionally adopt pure color generation as the atomic unit for evaluating Level-4 obedience. In contrast to complex compositional tasks where failures are often conflated with layout ambiguities or attribute-binding errors, pure color provides an unambiguous, pixel-perfect metric. Our rationale is that if a model lacks the systemic precision required to control a single, deterministic RGB value, it inherently fails at the most fundamental limit of instruction following. By isolating this “minimum viable obedience”, we provide a rigorous baseline for assessing deterministic control in generative AI.

**Inductive Bias and the “Aesthetic Inertia”.** Our empirical findings suggest that the obedience gap is not merely a consequence of data scarcity, but is deeply rooted in the inductive bias of current generative architectures. Standard training objectives—such as maximizing likelihood or minimizing reconstruction loss—naturally incentivize models to converge toward high-entropy manifold regions characterized by rich textures and complex semantics. Generating a pure color image (a zero-entropy state) requires the model to actively suppress these learned priors. This phenomenon, which we term “Aesthetic Inertia,” indicates that scaling data alone, without fundamental changes to architectural constraints or loss formulations, is unlikely to bridge the gap toward true Level-4 obedience.

**Benchmark Utility and Open-Sourcing.** To facilitate further exploration into the limits of AI controllability, we introduce the VIOLIN benchmark as a diagnostic tool for the community. VIOLIN is designed to be complementary to existing semantic-alignment benchmarks by focusing specifically on the deterministic precision of visual outputs. To support reproducibility and future research, we will release the complete VIOLIN suite, including our automated evaluation pipeline and dataset.